A model for the downstream evolution of temperate ice and subglacial hydrology along ice stream shear margins

Colin R. Meyer[1], Alissar Yehya[2], Brent Minchew[3], and James R. Rice[2,4]

[1]Department of Earth Sciences, University of Oregon, Eugene, OR, 97403 USA
[2]John A. Paulson School of Engineering and Applied Sciences, Harvard University, Cambridge, MA, 02138 USA
[3]Dept. of Earth, Atmospheric & Planetary Sciences, Massachusetts Institute of Technology, Cambridge, MA, 02139 USA
[4]Dept. of Earth and Planetary Sciences, Harvard University, Cambridge, MA, 02138 USA

Key Points:

- Along-flow variation in shear heating leads to generation of temperate ice along ice stream shear margins
- Shear heating in temperate ice produces meltwater that drains to the bed according to Darcy's law
- Temperate zone meltwater initiates a transition from distributed to channelized subglacial drainage

Corresponding author: Colin R. Meyer, colinrmeyer@gmail.com

Abstract

Antarctic mass balance and contribution to sea level rise are dominated by the flow of ice through narrow conduits called ice streams. These regions of relatively fast flow drain over 90% of the ice sheet and generate significant amounts of frictional heat at the ice stream margins where there is a transition to slow flow in the ridge. This heat can generate temperate ice and a sharp transition in flow speed between the stream and the ridge. Within zones of temperate ice, meltwater is produced and drains to the bed. Here we model the downstream development of a temperate zone along an ice stream shear margin and the flow of meltwater through temperate ice into a subglacial hydrologic system. The hydrology sets the basal effective pressure, defined as the difference between ice overburden and water pressure. Using the Southern shear margin of Bindschadler Ice Stream as a case study, our model results indicate an abrupt transition from a distributed to channelized hydrologic system within a few ice thicknesses of the point where the temperate zone initiates. This transition leads to a strengthening of the till due to reduced pore pressure because the water pressure in the channel is lower than in the distributed system, a potential mechanism by which hydrology can prevent lateral migration of shear margins.

1 Introduction

Ice streams drain 90% of the ice from the Antarctic Ice Sheet [*Bamber et al.*, 2000]. These narrow conduits of fast flow are often funneled through mountain valleys or along basal troughs and in this way are topographically controlled [*Truffer and Echelmeyer*, 2003]. In other places, however, topography does not dictate the lateral edges of ice streams. In the Siple Coast, for example, ice adjacent to ice streams, known as the ridge, flows slowly and is frozen to the bed [*Kamb*, 2001]. The large change in velocity between the ridge and the ice stream is accommodated in shear margins [*Raymond*, 1996]. Force balance requires the shear margins to sustain a high lateral shear stress in order to accommodate a large fraction of the gravitational driving stress because the weak basal sediments offer little resistive shear stress [*Whillans and Van Der Veen*, 1993, 1997; *Raymond et al.*, 2001]. Shearing in the margins can lead to a local decrease in the internal resistance to flow through two dominant processes: fabric development and shear heating. As ice is advected along the margin, ice crystals may align along flow and develop a fabric of preferential slip planes, which can lower the lateral shear stress supported by the margin [*Jacka and Budd*, 1989; *Jackson and Kamb*, 1997; *Minchew et al.*, 2018]. Simultaneously, heat induced by shearing can warm the ice, which softens the ice due to the viscosity dependence on temperature and meltwater. The net effect of these two processes can localize the shear margin to a region that is approximately an order of magnitude narrower than the ice stream width, where the ice in the margin has a much lower viscosity than the ice in the surrounding ridge and stream [*Echelmeyer et al.*, 1994; *Jacobson and Raymond*, 1998; *Schoof*, 2012]. Here we focus on the effects of ice softening in margins due to shear heating as fabric develops within the first few kilometers of a shear margin [*Jacka and Budd*, 1989; *Cuffey and Paterson*, 2010; *Minchew et al.*, 2018].

To study the thermomechanics of shear margins, *Perol and Rice* [2011, 2015] derive a one-dimensional temperature model including shear heating. When applied to shear margins in the Siple Coast, based on satellite-based deformation data summarized by *Joughin et al.* [2002], Perol and Rice find that it is common for shear margins to contain temperate ice, a binary mixture of ice and liquid water at the melting point, but the temperate zones are not necessarily continuous along the margins. This is consistent with the fact that ice streams rely in part on the inflow of ice from the surrounding cold ridges, suppressing the formation of temperate ice [*Suckale et al.*, 2014; *Haseloff et al.*, 2015]. Thus, the existence and thickness of a temperate zone must vary along the margin (Figure 1). For Bindschadler Ice Stream, *Perol and Rice* [2015] predict substantial temperate zones along the upstream margin (points TD1 and TD2, see Figure 2), whereas farther downstream, at points TD3 and D, they predict little to no temperate ice. The strain rate increases downstream of point D [*Scambos et al.*, 1994; *Elsworth and Suckale*, 2016] and, in section 3, we show that a substantial temperate zone develops.

Temperate ice supplies water to the bed, which affects the strength of basal sediments. In the Siple Coast, the underlying till is composed of water-saturated marine clay that deforms as a Coulomb-plastic material, where the yield stress depends linearly on the effective pressure, defined as the difference between the ice overburden and pore pressure [*Iverson et al.*, 1998; *Tulaczyk et al.*, 2000a; *Kamb*, 2001]. Below the centimeter-scale deforming region, the till is nearly impermeable and so the pore pressure is controlled by the drainage system at the ice-till interface [*Iverson and Iverson*, 2001]. Two conceptual modes of subglacial drainage at this interface are distributed and channelized. The effective pressure tends to be low (high pore pressure) in distributed drainage systems, potentially allowing the till to yield. On the other hand, the effective pressure is often higher in channels and, therefore, channelized drainage can strengthen the till, potentially making it less likely to yield. The increase in basal strength required in the transition from stream to ridge across a shear margin [*Kamb*, 2001; *Kyrke-Smith et al.*, 2013, 2015] is potentially due to channelization, as suggested by models [*Perol et al.*, 2015; *Elsworth and Suckale*, 2016; *Platt et al.*, 2016]. Observations also support channelized drainage along shear margins. *Vogel et al.* [2005] drilled into a cavity of flowing water (1.6 m vertical extent) in the shear margin of the stagnant Kamb Ice Stream, which is much larger than the millimeter-scale water films inferred by *Engelhardt and Kamb* [1997] and *Kamb* [2001]. Additionally, satellite observations show subglacially sourced meltwater channels on ice shelves are often collocated with shear margins [*Alley et al.*, 2016; *Marsh et al.*, 2016].

In this paper, we study the spatial evolution of temperate ice and subglacial hydrology along an ice stream shear margin. We examine the interaction between the water generated in the temperate zone and its influence on a subglacial hydrologic system. We start by describing a two-dimensional, steady state version of the *Schoof and Hewitt* [2016] model for englacial temperature as well as meltwater production and transport, that is able to represent the development of temperate ice zones through shear heating. We focus on how porosity and effective pressure evolve downstream in the temperate zone, treating the shear heating and advection velocities as data inputs to the model. Our model introduces the water that drains from the englacial system into the subglacial system and describes how the cumulative addition of water affects the state of the hydrologic system. We then apply these models to the southern shear margin of Bindschadler Ice Stream. Using velocity data collected from 2014-2015 [*Gardner et al.*, 2018], we show that the shear heating increases with downstream distance. We use this shear heating profile to determine the evolution of temperature, porosity, and englacial effective pressure as well as the basal effective pressure and style of drainage along the Bindschadler shear margin. We find a subglacial hydrologic system where distributed drainage transitions to channelized drainage downstream.

2 Theory

2.1 Temperate ice model

We model ice temperature within and along a two-dimensional downstream slice in the (x, z)-plane of an ice stream shear margin (Figure 1). The coordinate system is such that x is downstream, y is across the shear margin, and z is up, with $z = 0$ at the ice-bed interface and $z = H$ at the ice surface. Conservation of energy dictates that the evolution of temperature T

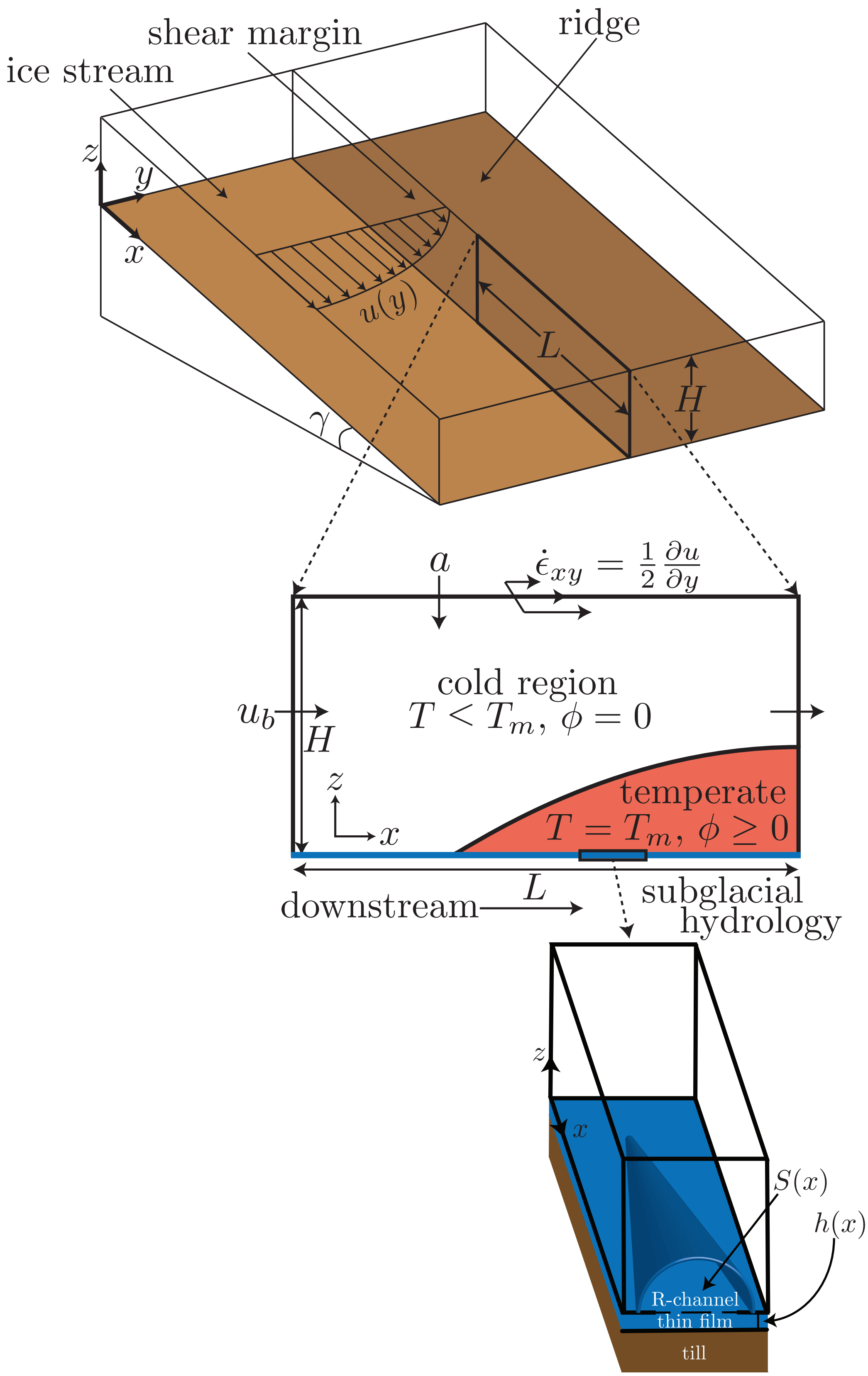

104 **Figure 1.** Schematic of an idealized ice stream shear margin, development of a temperate zone, and
105 the subglacial hydrology along an ice stream shear margin. The hydrology includes thin film and channel
106 drainage systems [after *Creyts and Schoof*, 2009; *Hewitt*, 2011, 2013].

in the shear margin is given as

$$\rho_I c_p \left(\frac{\partial T}{\partial t} + \boldsymbol{u}_I \cdot \boldsymbol{\nabla} T \right) = K \nabla^2 T + \sigma_{ij} \dot{\epsilon}_{ij} - \rho_w \mathscr{L} M, \tag{1}$$

where ρ_I is the ice density, ρ_w is the water density, c_p is the specific heat capacity, K is the thermal conductivity, and $\mathscr{L}$ is the specific latent heat. We treat these material properties as constants that are independent of time, space, and temperature (see Table 1). The ice velocity is $\boldsymbol{u}_I$, the meltrate is M, and the rate of heat production due to ice deformation is $\sigma_{ij}\dot{\epsilon}_{ij}$, where we employ the tensor summation convention. We use Glen's law for the rheology of ice, which is

$$\dot{\epsilon}_{ij} = A \tau_E^{n-1} \tau_{ij}, \tag{2}$$

where $\tau_{ij} = \sigma_{ij} + p\delta_{ij}$ is the deviatoric stress tensor, p is the pressure, δ_{ij} is the Kronecker delta, σ_{ij} is the Cauchy stress tensor, and $\dot{\epsilon}_{ij}$ is the strain rate tensor given by

$$\dot{\epsilon}_{ij} = \frac{1}{2} \left(\frac{\partial u_{Ii}}{\partial x_j} + \frac{\partial u_{Ij}}{\partial x_i} \right), \tag{3}$$

The effective stress τ_E and strain rate $\dot{\epsilon}_E$ are related as $\dot{\epsilon}_E = A\tau_E^n$, where the '$E$' subscript denotes the second variant of the respective tensor, *i.e.* $\dot{\epsilon}_E = \sqrt{\dot{\epsilon}_{ij}\dot{\epsilon}_{ij}/2}$. The parameters are A, which is the ice softness, and n is the rheological exponent [*Glen*, 1956; *Goldsby and Kohlstedt*, 2001; *Cuffey and Paterson*, 2010]. Thus, we compute the rate of heat generated by deforming ice $\sigma_{ij}\dot{\epsilon}_{ij}$ using Glen's law, Equation (2), as

$$\sigma_{ij}\dot{\epsilon}_{ij} = 2A^{-1/n} \dot{\epsilon}_E^{(n+1)/n}. \tag{4}$$

which is an important source of heat in shear margins where the dominant mode of deformation is lateral shear, *i.e.* $\dot{\epsilon}_E \approx \dot{\epsilon}_{xy}$ [*Joughin et al.*, 2002; *Schoof*, 2004; *Minchew et al.*, 2017]. Writing Equation (4) in this way allows us to determine the shear heating based on observed strain rates.

When the ice temperature is lower than the melting point, the meltrate M in Equation (1) is zero. The shear heating can warm the ice up to its melting temperature T_m to form temperate ice. Within the zone of temperate ice, the meltrate balances the heat generated by shearing, *i.e.* $\sigma_{ij}\dot{\epsilon}_{ij} = \rho_w \mathscr{L} M$. Meltwater runs along ice grain boundaries and collects at triple junctions where the ice grains intersect [*Nye and Frank*, 1973; *Mader*, 1992; *Lliboutry*, 1996]. Thus, the liquid water percolates through the ice grains as a porous media [*Hutter*, 1982; *Greve*, 1997; *Jordan and Stark*, 2001]. To model the evolution of the temperate region, we track the porosity ϕ, defined as the fractional volume of water in a given control volume.

Table 1. Table of parameters for the temperate ice, subglacial hydrology, and models.

temperate ice		subglacial hydrology		domain	
ρ_I	917 kg m^{-3}	f	0.04 m$^{4/3}$ kg$^{-1/2}$	L	6×10^4 m
c_p	2050 m^2 s^{-2} K^{-1}	u_b	10 m yr^{-1}	H	1000 m
$\mathscr{L}$	3.34×10^5 m^2 s^{-2}	r	0.002	T_m	273 K
K	2.1 kg m s^{-3} K^{-1}	m	3	T_s	247 K
g	9.806 m s^{-2}	G	0.06 kg s^{-3}	a	0.1 m yr^{-1}
A	2.4×10^{-24} Pa^{-3} s^{-1}	$\sin(\gamma)$	10^{-3}	N_{end}	10^5 Pa
n	3	w	10^4 m	Q_{in}	10^{-7} m^3 s^{-1}
κ_0	10^{-12} m^2	k_d	3.33×10^{-13}		
ν	7/3	α	4/3		
ρ_w	1000 kg m^{-3}	β	3/2		
η_w	10^{-3} Pa s	η_I	10^{13} Pa s		

Conservation of mass then dictates that

$$\frac{\partial \phi}{\partial t} + \boldsymbol{u}_I \cdot \boldsymbol{\nabla}\phi + \boldsymbol{\nabla} \cdot \boldsymbol{q} = M, \tag{5}$$

where $\boldsymbol{q}$ is the flux of water through the temperate ice and we ignore the minute amount of heat generated by the englacially flowing water [*Nye*, 1976; *Schoof and Hewitt*, 2016]. We model this flux using Darcy's law, given by

$$\boldsymbol{q} = -\frac{\kappa_0 \phi^\nu}{\eta_w} \left(\boldsymbol{\nabla} p_w + \rho_w g \hat{\boldsymbol{z}} \right) \tag{6}$$

where $\hat{\boldsymbol{z}}$ is the unit vector in the vertical direction, the viscosity of the water is η_w, and p_w is the water pressure. The permeability of the temperate ice is written as $\kappa_0 \phi^\nu$, a simplified version of the Carmen-Kozeny relationship, where κ_0 is the prefactor and ν is the porosity exponent.

We make two additional assumptions. First, we assume that the ice pressure is hydrostatic so $p_I = \rho_I g (H - z)$ for a constant ice thickness H, where the bed elevation is $z = 0$. We then define the effective pressure as the difference between the hydrostatic ice pressure and the meltwater pore pressure as

$$N = \rho_I g (H - z) - p_w. \tag{7}$$

Our second assumption is that the effective pressure N drives pore closure, thereby driving fluid flux, *i.e.*

$$\frac{\phi N}{\eta_I} = \boldsymbol{\nabla} \cdot \boldsymbol{q}, \tag{8}$$

with constant ice viscosity η_I [*Fowler*, 1984; *McKenzie*, 1984; *Schoof and Hewitt*, 2016]. The assumption of a constant ice viscosity is justified to the extent that the creep on the scale of grains is dominated by diffusional creep, the situation at low stress [*Frost and Ashby*, 1982]. Equations (7) and (8) allow us to determine the porosity and effective pressure within the temperate zone.

We construct a unified approach with a single evolution equation for the temperature and porosity in both the cold and temperate regions by writing the conservation of energy in terms of the specific enthalpy defined as

$$\mathscr{H} = \rho_I c_p (T - T_m) + \rho_w \mathscr{L} \phi, \tag{9}$$

which is the sum of sensible and latent heat contributions [*Aschwanden et al.*, 2012], where the water fully saturates the temperate ice [*Meyer and Hewitt*, 2017]. Neglecting the pressure dependence of the melting temperature T_m, we add Equations (1) and (5) using (8) and (9) to find an evolution equation for the enthalpy. We also combine Equations (6), (7), and (8) to write an equation for the effective pressure. These combined equations are given as

$$\frac{\partial \mathscr{H}}{\partial t} + \boldsymbol{u}_I \cdot \boldsymbol{\nabla} \mathscr{H} + \rho_w \mathscr{L} \frac{\phi N}{\eta_I} = K \nabla^2 T + \sigma_{ij} \dot{\epsilon}_{ij}, \tag{10}$$

$$\boldsymbol{\nabla} \cdot \left\{ \frac{\kappa_0 \phi^\nu}{\eta_w} \left[\boldsymbol{\nabla} N + (\rho_w - \rho_I) g \hat{\boldsymbol{z}} \right] \right\} = \frac{\phi N}{\eta_I}. \tag{11}$$

The values of the temperature T and porosity ϕ can be determined *a posteriori* from the enthalpy $\mathscr{H}$ using the inequalities

$$T = T_m + \min \left\{ \frac{\mathscr{H}}{\rho_I c_p}, 0 \right\}, \tag{12a}$$

$$\phi = \max \left\{ \frac{\mathscr{H}}{\rho_w \mathscr{L}}, 0 \right\}. \tag{12b}$$

The enthalpy approach has the advantage that the field is continuous across phase boundaries. At the temperate ice interface, the conditions on the interface are

$$\left[\rho_w \mathscr{L} \phi \left(\boldsymbol{u}_I - \dot{\boldsymbol{\xi}} \right) \right]^- \cdot \hat{\boldsymbol{n}} = [-K \boldsymbol{\nabla} T]^+ \cdot \hat{\boldsymbol{n}}, \tag{13a}$$

$$\boldsymbol{q} \cdot \hat{\boldsymbol{n}} = 0, \tag{13b}$$

$$T^- = T_m, \tag{13c}$$

where + indicates the cold ice region, − is within the temperate zone, $\dot{\boldsymbol{\xi}}$ is the velocity of the interface, and $\hat{\boldsymbol{n}}$ is the unit normal vector pointing out of the temperate zone [*Schoof and Hewitt*, 2016]. Equation (13a) is the Stefan condition at the cold-temperate interface and Equation (13b) enforces zero meltwater flux into the cold region. Additional discussion of the boundary conditions can be found in *Schoof and Hewitt* [2016].

On the exterior boundaries of the domain shown in Figure 1, we apply the conditions

$$T = T_s \quad \text{on} \quad z = H, \tag{14a}$$

$$T = T_m \quad \text{or} \quad N = N_b \quad \text{on} \quad z = 0 \tag{14b}$$

$$-K\boldsymbol{\nabla}T \cdot \hat{\boldsymbol{x}} = 0 \quad \text{on} \quad x = 0,\ L, \tag{14c}$$

where T_s is the surface temperature, N_b is the basal effective pressure set by the subglacial hydrologic system (section 2.2), and $\hat{\boldsymbol{x}}$ is the unit vector in the downstream direction.

We discretize these equations in space and time using a forward Euler, finite volume scheme implemented in MATLAB. The finite volume method is a conservative numerical method and, therefore, the conditions (13a) and (13b) are automatically enforced. Thus, the cold-temperate interface can be determined from the inequalities (12a) and (12b). We employ a relaxation method and thereby timestep the simulations to a steady state. Our mesh spacing is $dx = L/248$, $dy = H/128$ and we consider the simulation to be at steady state when the iteration difference error, defined as the sum of the squares of the differences divided by the average, is less than 10^{-8}. The code is included in the supplemental material.

2.2 Subglacial hydrology model

Along the shear margin, the ice-till interface receives water by *in situ* melting, upstream sources, and drainage from the overlying temperate ice. We model the hydrology at this interface using a one-dimensional downstream model that is invariant across the shear margin. Following *Hewitt* [2011], we describe the evolution of a thin film (distributed system) and a Röthlisberger channel [R-channel, *Röthlisberger*, 1972] with a semi-circular cross-section, see schematic in Figure 1 [*Creyts and Schoof*, 2009; *Kingslake and Ng*, 2013; *Kingslake*, 2015]. Both the R-channel and thin-film hydrologic systems evolve according to a balance between opening due to melting of ice or sliding and viscous creep closure. In this formulation, a channel only forms when there is too much water to be accommodated by the thin film, in which case, both systems operate simultaneously.

The thickness of the thin film h evolves according to

$$\frac{\partial h}{\partial t} = \frac{G}{\rho_I \mathscr{L}} + r u_b - \frac{h N_b}{\eta_I}, \tag{15}$$

where G is the geothermal heat flux, r is a dimensionless bed roughness, u_b is the basal sliding velocity. Thin film opening by sliding $r u_b$ is the product of two constants in our model (Table 1) and the effective pressure at the bed N_b varies with downstream distance. In general, the creep closure of the subglacial conduits can be written using the *Nye* [1953] solution and may include contributions from shearing within the margin [*Meyer et al.*, 2016, 2017]. However, we do not include the nonlinear *Nye* [1953] creep closure or shear softening and use a linear dependence on N_b following *Hewitt* [2011] as it contains the same physics and is consistent with the creep closure in the temperate ice. We also assume that the conduit closure rates are unaffected by the finite thickness of the overlying ice [*Evatt*, 2015]. The evolution of the cross-sectional area S of the R-channel is given by

$$\frac{\partial S}{\partial t} = \frac{Q_c \Psi}{\rho_I \mathscr{L}} - \frac{S N_b}{\eta_I}, \tag{16}$$

where Q_c is the flux of water through the channel and Ψ is the water pressure gradient defined as

$$\Psi = \rho_I g \sin(\gamma) + \frac{\partial N_b}{\partial x}, \tag{17}$$

and $\sin(\gamma)$ is the downstream slope of the ice surface and bed (Figure 1). Just as in the thermomechanical model, we include the time dependence for completeness in equation (16), yet only consider steady state solutions.

The total flux of water into the hydrologic system $Q(x)$ is the integral of the water entering the subglacial system from the temperate ice, *i.e.*

$$\frac{dQ}{dx} = w \boldsymbol{q} \cdot \hat{z} \quad \text{or equivalently} \quad Q(x) = w \int_0^x \boldsymbol{q} \cdot \hat{z} \, dx', \tag{18}$$

where w is the width of the shear margin and we assume the same flux into the subglacial system from the temperate ice across the shear margin, i.e. $\boldsymbol{q} \cdot \hat{z}$ is constant in the y-direction. We also ignore the small contributions from the ice melted within the subglacial system as well as melt generated by friction at the bed [*Hewitt*, 2011]. Mass conservation then partitions the available water into the distributed system and R-channel as

$$Q = Q_d + Q_c, \tag{19}$$

where we write the distributed flux Q_d as a generalized Poiseuille flow and use Darcy-Weisbach [*Chow*, 1959] to empirically describe the turbulent channelized flux Q_c, *i.e.*

$$Q_d = \frac{k_d h^3}{\eta_w}\Psi \tag{20a}$$

$$Q_c = f S^{\alpha} |\Psi|^{\beta-2}\,\Psi. \tag{20b}$$

The constant k_d describes the effective permeability of the distributed system, f is the friction factor that can be related to Manning roughness, thereby characterizing the roughness of the R-channel [*Clarke*, 1996], and the exponents α and β are empirical for turbulent flow.

In our formulation, water only enters the channel system if there is too much water be accommodated by the thin film. We define this transition based on the approximate distributed flux

$$\widetilde{Q}_d = \frac{k_d h^3}{\eta_w}\rho_I g \sin(\gamma), \tag{21}$$

where we neglect the small downstream gradient in effective pressure, *i.e.* $\Psi \approx \rho_I g \sin(\gamma)$ [*Hewitt*, 2011, 2013; *Werder et al.*, 2013]. This allows us to establish two regimes. In the first regime, the difference between the incoming flux and the approximate distributed flux is less than zero, *i.e.* $Q - \widetilde{Q}_d \leq 0$, and therefore, the hydrologic system is distributed only and no channel opens ($S = 0$). In the second regime, there is more water than the thin film system can accommodate, *i.e.* $Q - \widetilde{Q}_d > 0$ and so a channel opens ($S > 0$) with flux $Q_c = Q - \widetilde{Q}_d$. Neglecting the downstream gradient in effective pressure is reasonable everywhere except where the channel opens, but greatly simplifies the computations. Simulations where we did not neglect the downstream gradient yield nearly identical results and, we reiterate that the approximate distributed flux is only used to compute the transition location and determine the flux into the channelized system.

Combining all of these equations, we write the steady state system of equations as

$$\text{(total flux)} \qquad \frac{dQ}{dx} = w\boldsymbol{q}\cdot\hat{\boldsymbol{z}}, \tag{22}$$

$$\text{(transition flux)} \qquad \widetilde{Q}_d = \frac{k_d h^3}{\eta_w}\rho_I g \sin(\gamma), \tag{23}$$

$$\text{(flux switch)} \qquad Q = \begin{cases} \widetilde{Q}_d + f S^{\alpha}|\Psi|^{\beta-2}\Psi & \text{for} \quad Q > \widetilde{Q}_d \\ \dfrac{k_d h^3}{\eta_w}\Psi & \text{for} \quad Q \leq \widetilde{Q}_d \end{cases} \tag{24}$$

$$\text{(thin film)} \qquad hN_b = \frac{\eta_I G}{\rho_I \mathscr{L}} + \eta_I r u_b, \tag{25}$$

$$\text{(channel)} \qquad S^{\alpha-1}|\Psi|^{\beta} = \frac{\rho_I \mathscr{L}}{f\eta_I}N_b, \tag{26}$$

$$\text{(pressure)} \qquad \frac{dN_b}{dx} = \Psi - \rho_I g \sin(\gamma), \tag{27}$$

which we solve as a coupled system of ordinary differential equations in MATLAB using the boundary conditions

$$Q = Q_{\text{in}} \quad \text{at} \quad x = 0, \tag{28a}$$

$$N_b = N_{\text{end}} \quad \text{at} \quad x = L, \tag{28b}$$

where Q_{in} is the incoming flux from upstream and N_{end} is the effective pressure at the downstream end of the domain. The subglacial system is then coupled to the model for the englacial temperate ice by providing the basal boundary condition for the englacial effective pressure N, as in Equation (14b). The supplemental material contains our coded implementation.

3 Application to the southern Bindschadler shear margin

As a case study, we apply our model to the downstream region of the southern shear margin of Bindschadler Ice Stream, which is relatively straight, well-defined, and the shear strain rate increases with downstream distance, see Figure 2(a). This margin is part of the former suture zone with the now-stagnant Siple Ice Stream, a former distributary of Kamb Ice Stream [*Hulbe and Fahnestock*, 2007; *Catania et al.*, 2012; *Hulbe et al.*, 2016] that stagnated about 250 years before Kamb stagnated [*Retzlaff and Bentley*, 1993; *Smith et al.*, 2002; *Catania et al.*, 2003]. Topography does not appear to control the position of the Bindschadler/Siple shear margin and therefore it is a prototypical shear margin that is not topographically controlled.

Our model improves upon the downstream resolution and description of physical processes of prior models [*Scambos et al.*, 1994; *Joughin et al.*, 2004; *Elsworth and Suckale*, 2016]. We use the surface velocity fields derived from satellite imagery collected in 2014-2015 from Landsat 7 and 8, which are provided with 240-m spatial resolution [*Gardner et al.*, 2018], to calculate the lateral shear strain rate along the margin. We model the development of temperate ice along flow using Equations (10)-(11) and couple it to the subglacial hydrologic model described in Equations (22)-(27). We compute the shear heating $\sigma_{ij}\dot{\epsilon}_{ij}$ that occurs along the margin from Equation (4) and approximate the effective strain rate as $\dot{\epsilon}_E \approx \dot{\epsilon}_{xy}$ because downstream shear is the dominant strain rate in the margin. We use the strain rates along ∼55 km of the downstream southern shear margin calculated from observed velocity fields [*Gardner et al.*, 2018]. The strain rate along this margin increases quasi-linearly with distance, as shown in Figure 2(b), thus, we represent the data parametri-

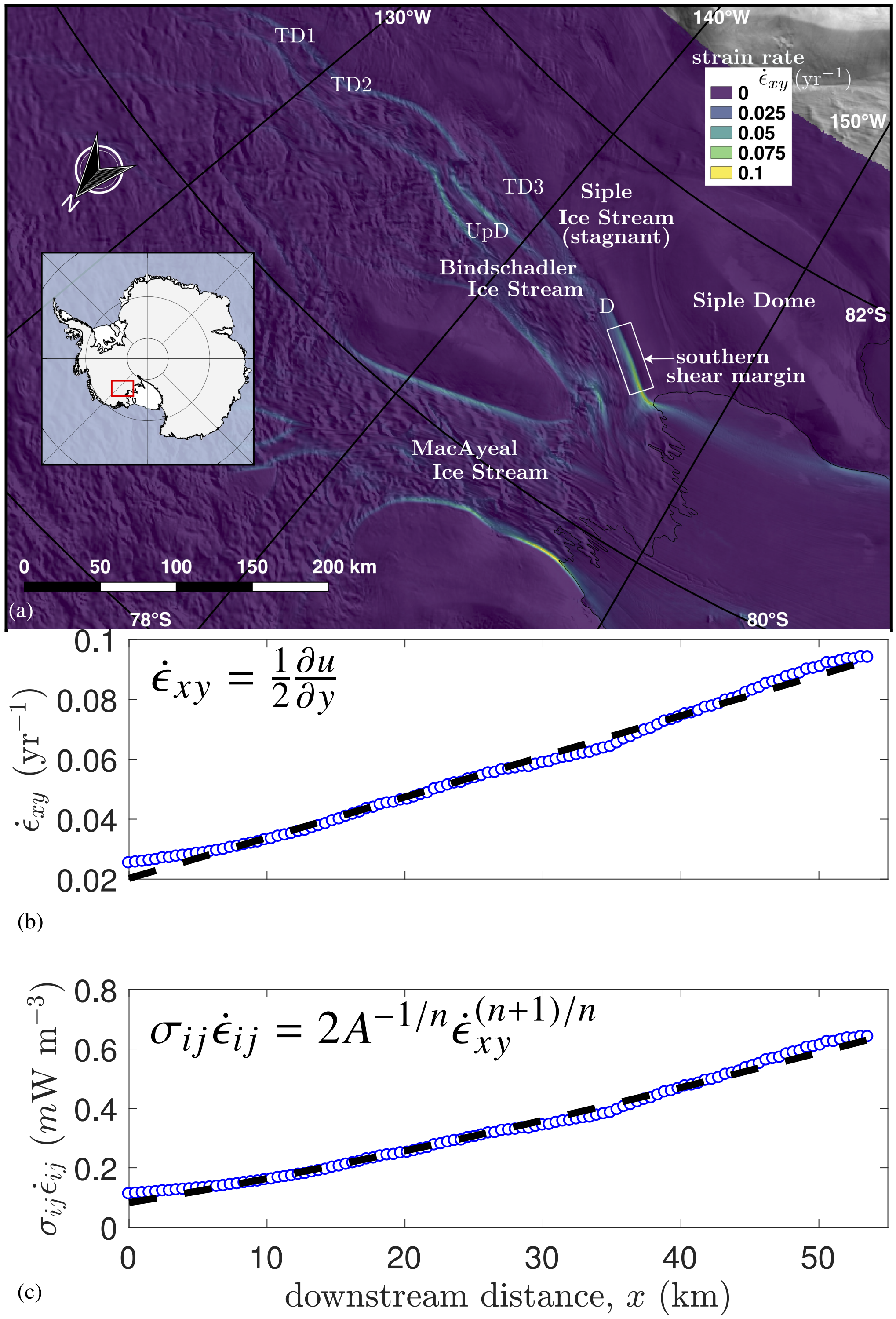

Figure 2. Observed strain rates in MacAyeal and Bindschadler Ice Streams: (a) Map of lateral shear strain rates calculated from observed surface velocities [*Gardner et al.*, 2018] overlying the MODIS mosaic of Antarctica [*Scambos et al.*, 2007]. (b) Strain rate and (c) shear heating development along the southern Bindschadler shear margin compared with the parametrized lines (where every fifth data point is plotted for clarity).

cally as

$$\dot{\epsilon}_{xy} = \left(0.0741\ \mathrm{yr}^{-1}\right)\frac{x}{L} + 0.0202\ \mathrm{yr}^{-1} \tag{29}$$

which is shown with a black dashed line in Figure 2(b). We compute the shear heating by inserting Equation (29) into Equation (4). The ice softness A is strongly temperature T and porosity ϕ dependent and is a function of the ice crystal orientation [*Duval*, 1977; *Paterson*, 1977; *Cuffey and Paterson*, 2010]. We, however, take A to be constant and equal to the value expected for temperate ice, which allows us to estimate the shear heating from the data. Evaluating A at the melting temperature, moreover, represents the minimum expected shear heating excluding the effects of fabric and porosity. Thus, our model results are robust to this simplification.

For ice advection, we consider constant velocity as

$$\boldsymbol{u}_I = (u_b, 0, -a) \tag{30}$$

where u_b is a representative downstream velocity for the shear margin and the vertical velocity is given by the surface accumulation rate a. The downstream velocity varies only slightly with distance and for the vertical velocity we ignore the variation with depth as the accumulation rate is small [Table 1; *Schoof and Hewitt*, 2016]. A vertically uniform velocity also gives the minimum thickness for the temperate zone as a height-dependent velocity would only decrease the amount of cold ice advected into the temperate zone. We neglect lateral flow across the margin as inflow from Siple Dome is slow (≈1 m/yr) and not enough time has elapsed since the stagnation of Siple Ice Stream for ice to flow across and influence the Bindschadler/Siple shear margin [*Nereson*, 2000]. In this way, we assume that the shear margin is in steady state with respect to downstream flow and unaffected by lateral inflow.

With the shear heating and ice advection specified, we now solve the enthalpy and effective pressure equations, *i.e.* Equations (10) and (11), subject to the boundary conditions (14a)–(14c), in the rectangular domain of Figure 1. The steady state simulations for the temperature, porosity, and effective pressure fields are shown in Figure 3. As expected, the temperature field, Figure 3(a), shows that the increase in shear heating with downstream distance leads to an increase in temperature within the ice column. Then, at approximately 20 km downstream along the southern shear margin, a zone of temperate ice emerges. The cold-temperate boundary is shown on the figure as a solid black line. Within the temperate ice the porosity and effective pressure develop downstream, as shown in Figures 3(b) and 3(c). The porosity is zero at the cold-temperate boundary and generally increases with depth and dis-

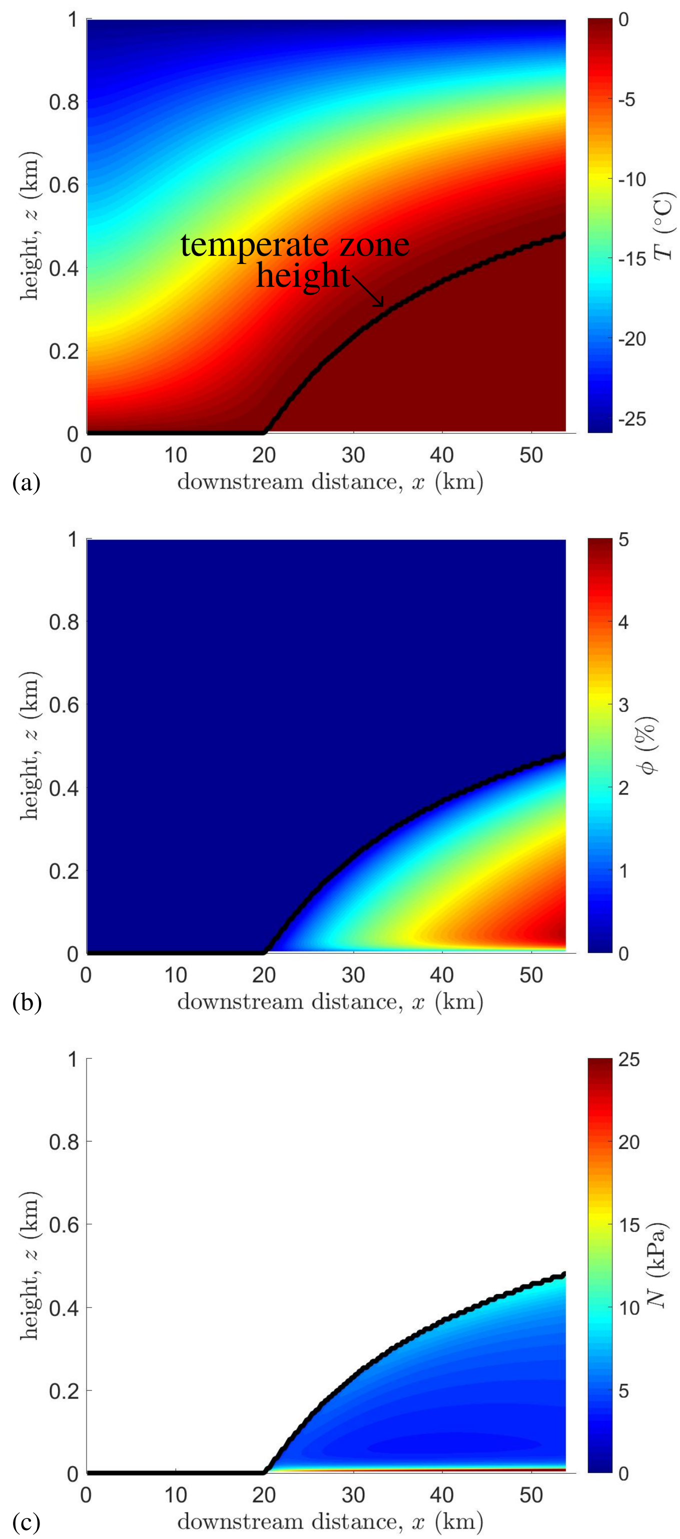

Figure 3. Evolution of a temperate zone with downstream distance along the southern margin of Bindschadler Ice Stream: (a) Temperature increases with downstream distance. (b) Porosity increases with downstream and vertically. (c) Effective pressure varies with downstream distance and is largest at the interface between the temperate ice and subglacial hydrologic system.

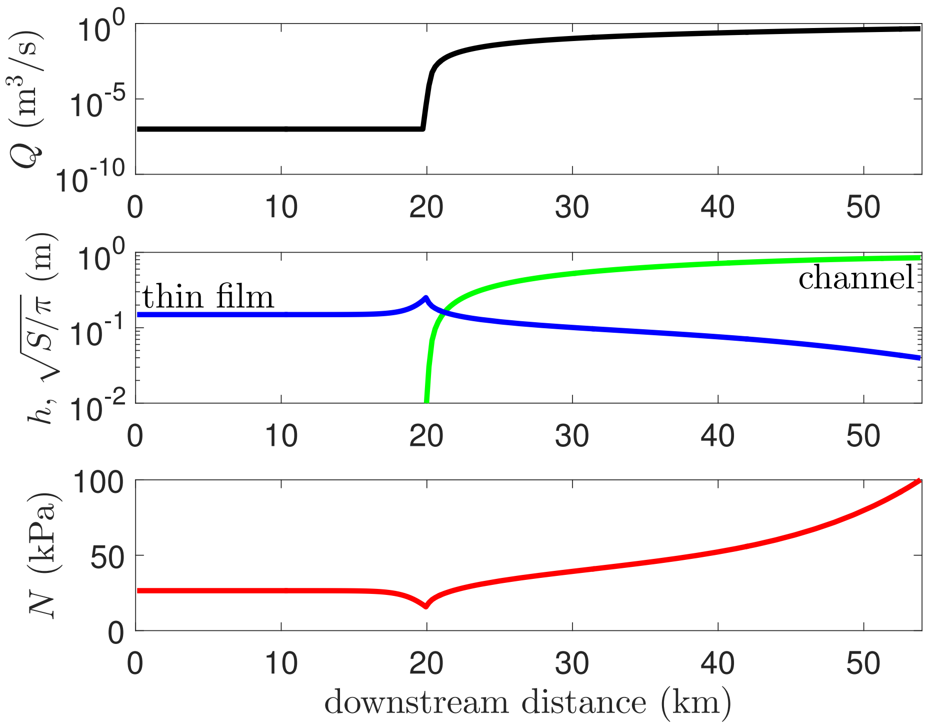

Figure 4. Results of the coupled temperate ice and subglacial hydrology models: (top panel) flux out of the temperate zone into the subglacial system. (middle panel) size of subglacial conduits as a function of downstream distance. The water that drains from the temperate ice quickly overwhelms the distributed system and channelization occurs. (bottom panel) subglacial effective pressure with downstream distance showing a transition from distributed to channelized drainage.

tance downstream. When ice flows into a temperate zone, as is true in this case, the porosity must o to zero at the cold-temperate boundary. However, this is not the case when the ice flows out from the temperate zone into a cold region, where a jump in porosity is possible as it is balanced by refreezing at the interface [*Schoof and Hewitt*, 2016]. The effective pressure is undefined in the cold region where there is no liquid water and is relatively large at the cold-temperate boundary. At the bottom of the domain, the subglacial effective pressure induces a very large effective pressure within the ice. This large englacial effective pressure leads to compaction of the ice by Equation (8) and a low-porosity layer develops near the bottom of the domain in Figure 3(b).

The evolution of the temperature field and development of a temperate zone is coupled to the evolution of the subglacial hydrologic system. Figure 4 shows subglacial effective pressure with downstream distance and the flux of water entering the subglacial system from the overlying temperate ice, for a single set of parameters (Table 1). We show how the variation of parameters affects the effective pressure distribution in the next section, Figures 5 and 6, but the trends are equivalent. The results in Figure 4(b) show that there is a transition from distributed to channelized drainage with downstream distance. This transition indicates that the width-averaged subglacial hydrologic system changes from an entirely distributed system to a thin film and channel system where the effective pressure in the margin is governed by the channel. In the region upstream of where the temperate zone initiates, *i.e.* $x < 20$ km, the hydrology is distributed ($S = 0$) and the thin-film size is given as a balance between geothermal heat as well as sliding and ice creep closure (Equation (15)). As soon as the temperate zone initiates, the water entering the distributed system from the temperate ice leads to a rapid increase in the thin-film thickness, at which point there is enough water to open an R-channel (Figure 4(b)). At the same time as the flux through the thin-film system increases, the effective pressure decreases (Figure 4(a)), which is the well-known feature of distributed systems that the flux and effective pressure are inversely proportional [*Fowler*, 2011]. Once the channelized system initiates, the effective pressure increases to N_{end}, the applied downstream boundary condition. The radius of the channel grows with downstream distance, while the thin-film thickness decreases.

4 Discussion

Our results show the evolution of a temperate zone along an ice stream shear margin. In our model, this comes from a one-way thermomechanical coupling where the increase in lateral shear strain rate leads to an increase in shear heating and therefore the growth of a temperate zone. In general, however, there is a nonlinear two-way coupling between shear heating and viscosity within a shear margin whereby the warming of ice and development of temperate ice increases the lateral shear strain rate and the ice softness A while decreasing the width of the shear margin and the lateral shear stress [*Schoof and Hewitt*, 2013]. This results in a narrow shear margin composed of warm, soft ice. Although, we use the value of ice softness evaluated at the melting temperature in our computations, our results indicate significant downstream softening of ice in shear margins.

The generation of meltwater within the temperate zone also softens the ice, and the water that drains from the temperate ice influences subglacial hydrology. We find that the extra water supplied by the temperate ice leads to a transition from a thin-film distributed system

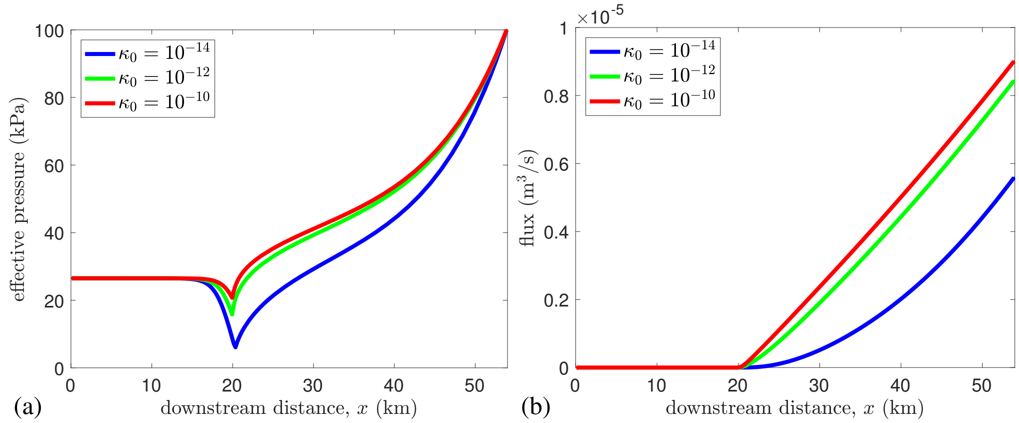

Figure 5. Variation of the permeability of temperate ice κ_0 and its effect on (a) effective pressure and (b) flux of water into the subglacial system.

to channelized drainage within a few ice thicknesses downstream from the onset of the temperate zone along the southern shear margin. This evolution of the subglacial hydrologic system corroborates *Elsworth and Suckale* [2016], who use a sequence of (y, z)-slices along the same Bindschadler margin and conceptualize a transition from distributed to channelized drainage. This transition occurs in our model partly because of the low permeability of our thin-film distributed system. For the permeability prefactor k_d in Equation (20a), we use $k_d = 3.33 \times 10^{-13}$, a value that leads to a permeability that is similar in order of magnitude to the estimates for subglacial till and much smaller than typical thin film systems [*Fountain and Walder*, 1998; *Tulaczyk et al.*, 2000a; *Kamb*, 2001]. The low permeability is comparable to the thin-film model of *Perol et al.* [2015]. Our modeling results suggest that the thin-film conduits under ice streams are likely centimeter-scale regions of porous deforming till [*Iverson and Iverson*, 2001].

To understand how the parameter choices affect our results, we vary five parameters: the englacial permeability prefactor κ_0 (Figure 5), the distributed drainage permeability k_d, the incoming flux from upstream Q_{in}, the downstream effective pressure N_{end}, and the R-channel friction factor f (Figure 6). Starting with the variation of the temperate ice permeability, we can see that κ_0 affects the subglacial effective pressure (Figure 5(a)) and amount of water that leaves the temperate zone and enters the subglacial system (Figure 5(b)). The largest permeability leads to the largest flux of water into the subglacial system (red lines in Figure 5(a) and (b)). The lowest permeability has the lowest flux into the subglacial system

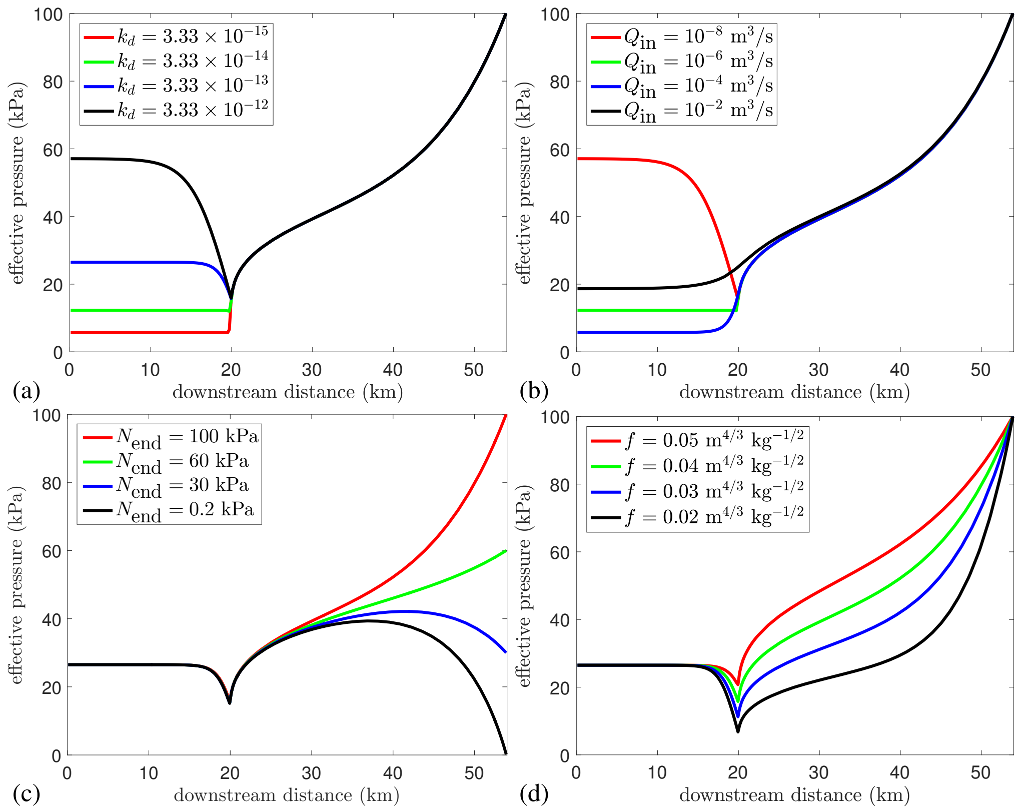

Figure 6. Variation of the (a) permeability of the distributed drainage system k_d; (b) incoming flux of water from upstream Q_{in} (black line is channelized throughout); (c) downstream effective pressure boundary condition N_{end}; and (d) friction resistance within the R-channel f. The flux of water into the subglacial system from the temperate ice is the same in all cases.

and the transition from distributed to channelized drainage occurs at the most downstream point. While the effective pressure and flux do respond quantitatively to a variation in κ_0, the qualitative features remain unchanged. In other words, a four orders of magnitude change in the value of κ_0, leads to a change in the position of distributed-to-channelized transition of a few kilometers and the flux changes by less than a factor of two.

Changing the permeability of the distributed system k_d (without changing the flux of water into the subglacial system), as shown in Figure 6(a), also affects the subglacial effective pressure. In the region upstream of the temperate zone, the distributed subglacial hydrology model reduces to

$$h = \left(\frac{\eta_w Q_{\text{in}}}{k_d \rho_I g \sin(\gamma)}\right)^{1/3}, \tag{31}$$

$$N_b = \left(\frac{\eta_I G}{\rho_i \mathscr{L}} + \eta_I r u_b\right)\left(\frac{k_d \rho_I g \sin(\gamma)}{\eta_w Q_{\text{in}}}\right)^{1/3}. \tag{32}$$

Thus, as the permeability k_d increases, the thin film thickness decreases, leading to an increase in the basal effective pressure, which is shown in Figure 6(a). Following the same logic, increasing the flux of water from upstream decreases the effective pressure in the distributed system until, for a large enough incoming flux, a channelized drainage system exists along the entire shear margin (black line in Figure 6(b)). The incoming water from the temperate zone prevents the hydrologic system from staying distributed throughout the domain. Varying the downstream effective pressure N_{end}, however, does not affect the distributed effective pressure nor does it change the location of the transition between the drainage systems. If the end of the domain is near the grounding line (black line in Figure 6(c)), there is a small increase in the effective pressure after the distributed-to-channelized transition and then a decrease to low effective pressure over about ten kilometers. As we decrease the frictional resistance in the channel, the effective pressure drops and then increases sharply to satisfy the N_{end} boundary condition.

Considering a force balance on the ice stream, the development of temperate ice by shear heating weakens the lateral shear stress exerted by the margins. Thus, in the absence of lateral control on margin position, the bed in the margin must strengthen or cold ice must advect in from the ridge in order to counteract the driving stress [*Jacobson and Raymond*, 1998; *Suckale et al.*, 2014; *Haseloff et al.*, 2015]. The inflow of cold ice from the ridge, or equivalently margin migration in the frame of the margin, can extinguish the temperate ice and increase the lateral shear stress [*Perol and Rice*, 2015]. For a steady margin position, the bed must strengthen, which is consistent with our results showing a transition in subglacial hydrology from distributed to channelized drainage leading to an increase in basal effective pressure. Assuming that in the vicinity of the ice stream the dominant mechanism of glacier motion is due to plastic yielding of water saturated till, we equate the basal shear stress with the local till yield stress [*Iverson et al.*, 1998; *Tulaczyk et al.*, 2000b; *Minchew et al.*, 2016]. From a Mohr-Coulomb yield criterion, we can relate the basal shear stress (now equivalent to the till yield stress) to the effective pressure in the till as

$$\tau_b = \tan(\varphi)N, \tag{33}$$

where we assume that $\tan(\varphi) = 0.4$ and cohesion is negligible [*Rathbun et al.*, 2008]. In this way, the strength of the sediments is directly proportional to the effective pressure. For many parameter combinations, the effective pressure is lower (*i.e.* the till is likely weaker) in the upstream part of the margin, where the drainage system is distributed, than far downstream where the hydrologic system is channelized. In the immediate vicinity of the transition point, the effective pressure drops precipitously and, after the transition, the growth of the channel may require one to twenty kilometers for the effective pressure to increase beyond that of the distributed system.

A mechanism for preventing a shear margin from migrating laterally through channelized subglacial hydrology is presented in *Perol et al.* [2015], which contains a similar subglacial system to the *Creyts and Schoof* [2009] hydrologic system utilized by *Kyrke-Smith et al.* [2013, 2015] to obtain stable shear margins. In this paper, we have deliberately avoided lateral drainage but note that it could be easily incorporated as a drainage sink that will likely depend on the drainage configuration. A freezing till mechanism for stable shear margins is postulated by *Jacobson and Raymond* [1998], *Schoof* [2012], and *Haseloff et al.* [2015], but we do not delve into a frozen fringe description [*Rempel et al.*, 2004; *Rempel*, 2008, 2009]. Rather, we summarize the basic mechanism by which a channel can lock a shear margin. In a (y, z)-cross-section across a shear margin the till is frozen under the ridge and shearing under the stream [*Schoof*, 2004; *Perol et al.*, 2015]. Thus, the transition between frozen and deforming till is analogous to the tip of a mode-III (tearing) crack, where there is a stress concentration at the transition point [*Rice*, 1967, 1968; *Schoof*, 2004]. If the stress at the transition point is larger than the till yield stress, the failed till region will advance and the ice stream will widen. An R-channel provides a mechanism to lock the margin in place by strengthening the till and reducing the stress concentration below the yield stress of the till [*Perol et al.*, 2015; *Meyer et al.*, 2016; *Platt et al.*, 2016].

While we use data from the southern Bindschadler shear margin, the development of temperate ice and the formation of subglacial channels are general results that can be applied to any active shear margin that is underlain by till of low permeability and not controlled by topography. Two examples of locations where our results may be insightful are the eastern shear margin of Thwaites Glacier [*MacGregor et al.*, 2013; *Schroeder et al.*, 2013, 2016] and the margins of Whillans Ice Stream [*Anandakrishnan et al.*, 1998; *Suckale et al.*, 2014; *Perol et al.*, 2015]. Using radar backscatter data, *Peters et al.* [2005] find a sharp transition in bed reflectivity across the Dragon margin on the Whillans Ice Stream, which they interpret as an abrupt change in subglacial hydrology, consistent with the *Perol et al.* [2015] model. On the other hand, *Raymond et al.* [2006] do not observe a significant jump in bed reflectivity in the upstream region of the same Whillans shear margin. Similarly, *MacGregor et al.* [2013] do not see a large change in bed reflectivity across the eastern shear margin of Thwaites Glacier. They invoke distributed drainage as a possible mechanism, which may be indicative of an unstable margin.

5 Conclusions

In this paper we describe the coupled development of temperate ice and subglacial hydrology along an ice stream shear margin. We force our thermomechanical model using observed shear strain rates to compute the shear heating within the shear margin. We use a surface velocity field derived from Landsat 7-8 satellite imagery [*Gardner et al.*, 2018] to obtain high-resolution strain rate data along the southern Bindschadler shear margin, from which we compute the shear heating along the margin. In our thermomechanical model, we use an enthalpy formulation to compute the englacial ice temperature in both the cold region, where the ice is below the melting point, and the temperate zone. Meltwater generated in the temperate zone flows through the porous ice, driven by gradients in the englacial effective pressure, and enters a subglacial hydrologic system. At the upstream end of our domain, the subglacial system is distributed and the effective pressure is low. Downstream of where the temperate zone emerges, the englacially sourced water initiates a channel and the high effective pressure in the channel strengthens the sediments and locks the margin in a stable configuration. In this way, our model shows that ice stream shear margins develop temperate ice downstream and their lateral migration is stabilized by channelized drainage.

The development of subglacial hydrology along the shear margin, *i.e.* the transition from distributed to channelized drainage shows that shear margins are not uniformly susceptible to lateral migration. Appealing to the stability mechanism of *Perol et al.* [2015], the portions of the margin where there is a distributed subglacial system are more likely to migrate than where there is a channelized drainage. This is visible in Figure 2: the upper part of the southern Bindschadler shear margin is diffuse whereas the downstream margin is straight, well-defined, and shear strain rate increases downstream. Additionally, *MacGregor et al.* [2013] propose that the hydrology below the eastern shear margin of Thwaites Glacier may be a distributed system due to the small change in bed reflectivity, which could make the margin susceptible to lateral migration.

Furthermore, when a temperate zone develops in a shear margin it remains for a long time, even if the forcing is removed, because advection and diffusion are processes with timescales on the order of 10 kyr. Thus, even though new melt will not be produced after the stagnation of an ice stream, water will continue to drain from the temperate ice in the shear margin to the bed. *Vogel* [2004] observe channelized flow in the margin of the stagnated Kamb Ice Stream, which is potentially sourced from relic temperate ice within the margin. This does not rule out water piracy as a mechanism for stagnation [*Alley et al.*, 1994; *Anandakrishnan and Alley*, 1997] but rather highlights the importance of hydrology in shear margins.

Acknowledgments

We wish to thank Timothy Creyts, Ian Hewitt, Thibaut Perol, Alan Rempel, and Jenny Suckale for insightful discussions. We would also like to thank the Associate Editor Olga Sergienko, an anonymous reviewer, Geoff Evatt, and Jonny Kingslake for comments. The data used in this paper is either publicly available or can be generated using the code appended in the supplement. The code can also be found on GitHub with DOI: 10.5281/zenodo.1288804. We are grateful for the support of the NSF Graduate Research Fellowship award DGE1144152 and a David Crighton Fellowship to CRM, the NSF Office of Polar Programs grant number PP1341499 (JRR), and the NSF Earth Sciences Postdoctoral Fellowship award EAR1452587 (BM).

References

Alley, K. E., T. A. Scambos, M. R. Siegfried, and H. A. Fricker (2016), Impacts of warm water on Antarctic ice shelf stability through basal channel formation, *Nat. Geosci.*, *9*(4), 290–293, doi:10.1038/ngeo2675.

Alley, R. B., S. Anandakrishnan, C. R. Bentley, and N. Lord (1994), A water-piracy hypothesis for the stagnation of Ice Stream C, Antarctica, *Ann. Glaciol.*, *20*(1), 187–194, doi: 10.1017/S0260305500016438.

Anandakrishnan, S., and R. B. Alley (1997), Stagnation of ice stream C, West Antarctica by water piracy, *Geophysical Research Letters*, *24*(3), 265–268, doi:10.1029/96GL04016.

Anandakrishnan, S., D. Blankenship, R. Alley, and P. Stoffa (1998), Influence of subglacial geology on the position of a West Antarctic ice stream from seismic observations, *Nature*, *394*(6688), 62–65, doi:10.1038/27889.

Aschwanden, A., E. Bueler, C. Khroulev, and H. Blatter (2012), An enthalpy formulation for glaciers and ice sheets, *J. Glaciol.*, *58*(209), 441–457, doi:10.3189/2012JoG11J088.

Bamber, J. L., D. G. Vaughan, and I. Joughin (2000), Widespread complex flow in the interior of the Antarctic ice sheet, *Science*, *287*(5456), 1248–1250, doi: 10.1126/science.287.5456.1248.

Catania, G., C. Hulbe, H. Conway, T. A. Scambos, and C. F. Raymond (2012), Variability in the mass flux of the ross ice streams, West Antarctica, over the last millennium, *J. Glaciol.*, *58*(210), 741–752, doi:10.3189/2012JoG11J219.

Catania, G. A., H. B. Conway, A. M. Gades, C. F. Raymond, and H. Engelhardt (2003), Bed reflectivity beneath inactive ice streams in West Antarctica, *Ann. Glaciol.*, *36*(1), 287–291, doi:10.3189/172756403781816310.

Chow, T. V. (1959), *Open channel hydraulics*, McGraw-Hill.

Clarke, G. K. C. (1996), Lumped-element analysis of subglacial hydraulic circuits, *J. Geophys. Res.*, *101*(B8), 17,547–17,559, doi:10.1029/96JB01508.

Creyts, T. T., and C. Schoof (2009), Drainage through subglacial water sheets, *J. Geophys. Res.*, *114*(F04008), 1–18, doi:10.1029/2008jf001215.

Cuffey, K. M., and W. S. B. Paterson (2010), *The Physics of Glaciers (Fourth Edition)*, ISBN 9780123694614, Elsevier.

Duval, P. (1977), The role of the water content on the creep rate of polycrystalline ice, *IAHS*, *118*, 29–33.

Echelmeyer, K. A., W. D. Harrison, C. Larsen, and J. E. Mitchell (1994), The role of the margins in the dynamics of an active ice stream, *J. Glaciol.*, *40*(136), 527–538, doi: 10.3198/1994JoG40-136-527-538.

Elsworth, C. W., and J. Suckale (2016), Rapid ice flow rearrangement induced by subglacial drainage in West Antarctica, *Geophys. Res. Lett.*, *43*(22), 697–707, doi:

10.1002/2016GL070430.

Engelhardt, H. F., and B. Kamb (1997), Basal hydraulic system of a West Antarctic ice stream: Constraints from borehole observations, *J. Glaciol.*, *43*(144), 207–230, doi: 10.1017/S0022143000003166.

Evatt, G. W. (2015), Röthlisberger channels with finite ice depth and open channel flow, *Ann. Glaciol.*, *50*(70), 45–50, doi:10.3189/2015aog70a992.

Fountain, A. G., and J. S. Walder (1998), Water flow through temperate glaciers, *Rev. Geophys.*, *36*, 299–328, doi:10.1029/97rg03579.

Fowler, A. (2011), *Mathematical geoscience*, vol. 36, Springer Science & Business Media.

Fowler, A. C. (1984), On the transport of moisture in polythermal glaciers, *Geophys. Astrophys. Fluid Dyn.*, *28*(2), 99–140, doi:10.1080/03091928408222846.

Frost, H. J., and M. F. Ashby (1982), *Deformation mechanism maps: the plasticity and creep of metals and ceramics*, Pergamon Press.

Gardner, A. S., G. Moholdt, T. Scambos, M. Fahnstock, S. Ligtenberg, M. van den Broeke, and J. Nilsson (2018), Increased West Antarctic and unchanged East Antarctic ice discharge over the last 7 years, *Cryosphere*, *12*(2), 521–547, doi:10.5194/tc-12-521-2018.

Glen, J. W. (1956), Measurement of the deformation of ice in a tunnel at the foot of an ice fall, *J. Glaciol.*, *2*(20), 735–745, doi:10.3198/1956JoG2-20-735-746.

Goldsby, D., and D. Kohlstedt (2001), Superplastic deformation of ice: Experimental observations, *J. Geophys. Res.*, *106*, 11,017–11,030, doi:10.1029/2000jb900336.

Greve, R. (1997), A continuum–mechanical formulation for shallow polythermal ice sheets, *Philos. Trans. R. Soc. London, Ser. A*, *355*(1726), 921–974, doi:10.1098/rsta.1997.0050.

Haseloff, M., C. Schoof, and O. Gagliardini (2015), A boundary layer model for ice stream margins, *J. Fluid Mech.*, *781*, 353–387, doi:10.1017/jfm.2015.503.

Hewitt, I. J. (2011), Modelling distributed and channelized subglacial drainage: the spacing of channels, *J. Glaciol.*, *57*(202), 302–314, doi:10.3189/002214311796405951.

Hewitt, I. J. (2013), Seasonal changes in ice sheet motion due to melt water lubrication, *Earth Planet. Sci. Lett.*, *371*, 16–25, doi:10.1016/j.epsl.2013.04.022.

Hulbe, C., and M. Fahnestock (2007), Century-scale discharge stagnation and reactivation of the Ross ice streams, West Antarctica, *J. Geophys. Res.*, *112*(F3), doi: 10.1029/2006JF000603.

Hulbe, C. L., T. A. Scambos, M. Klinger, and M. A. Fahnestock (2016), Flow variability and ongoing margin shifts on Bindschadler and MacAyeal Ice Streams, West Antarctica, *J.*

Geophys. Res., *121*(2), 283–293, doi:10.1002/2015JF003670, 2015JF003670.

Hutter, K. (1982), A mathematical model of polythermal glaciers and ice sheets, *Geophys. Astrophys. Fluid Dyn.*, *21*(3-4), 201–224, doi:1080/03091928208209013.

Iverson, N. R., and R. M. Iverson (2001), Distributed shear of subglacial till due to Coulomb slip, *J. Glaciol.*, *47*(158), 481–488, doi:10.3189/172756501781832115.

Iverson, N. R., T. S. Hooyer, and R. V. V. Baker (1998), Ring-shear studies of till deformation: Coulomb-plastic behavior and distributed strain in glacier beds, *J. Glaciol.*, *44*(148), 634–642, doi:10.3198/1998JoG44-148-634-642.

Jacka, T. H., and W. F. Budd (1989), Isotropic and anisotropic flow relations for ice dynamics, *Ann. Glaciol.*, *12*(1), 81–84, doi:10.3189/1989AoG12-1-81-84.

Jackson, M., and B. Kamb (1997), The marginal shear stress of Ice Stream B, West Antarctica, *J. Glaciol.*, *43*(145), 415–426, doi:10.3198/1997JoG43-145-415-426.

Jacobson, H. P., and C. F. Raymond (1998), Thermal effects on the location of ice stream margins, *J. Geophys. Res.*, *103*(B6), 12,111–12,122, doi:10.1029/98JB00574.

Jordan, R., and J. Stark (2001), Capillary Tension in Rotting Ice Laters, *Tech. rep.*, Technical Report ERDC/CRREL TR-01-13. US Army Corps of Engineers, Cold Regions Research and Engineering Laboratory.

Joughin, I., S. Tulaczyk, R. Bindschadler, and S. F. Price (2002), Changes in West Antarctic Ice Stream velocities: Observation and analysis, *J. Geophys. Res.*, *107*(B11), doi: 10.1029/2001JB001029.

Joughin, I., D. R. MacAyeal, and S. Tulaczyk (2004), Basal shear stress of the Ross ice streams from control method inversions, *J. Geophys. Res.*, *109*(B9), 1–20, doi: 10.1029/2003JB002960.

Kamb, B. (2001), Basal zone of the West Antarctic Ice Streams and its role in lubrication of their rapid motion, in *The West Antarctic Ice Sheet: Behavior and Environment*, vol. 77, edited by R. B. Alley and R. A. Bindschadler, pp. 157–199, AGU, Washington, DC, doi: 10.1029/ar077p0157.

Kingslake, J. (2015), Chaotic dynamics of a glaciohydraulic model, *J. Glaciol.*, *61*(227), 493–502.

Kingslake, J., and F. Ng (2013), Modelling the coupling of flood discharge with glacier flow during jökulhlaups, *Ann. Glaciol.*, *54*(63), 25–31, doi:10.3189/2013aog63a331.

Kyrke-Smith, T. M., R. F. Katz, and A. C. Fowler (2013), Subglacial hydrology and the formation of ice streams, *Proc. R. Soc. Lond. Ser. A*, *470*(2161), doi:10.1098/rspa.2013.0494.

Kyrke-Smith, T. M., R. F. Katz, and A. C. Fowler (2015), Subglacial hydrology as a control on emergence, scale, and spacing of ice streams, *J. Geophys. Res.*, *120*(8), 1501–1514, doi:10.1002/2015JF003505, 2015JF003505.

Lliboutry, L. (1996), Temperate ice permeability, stability of water veins and percolation of internal meltwater, *J. Glaciol.*, *42*(141), 201–211, doi:10.3198/1996JoG42-141-201-211.

MacGregor, J. A., G. A. Catania, H. Conway, D. M. Schroeder, I. Joughin, D. A. Young, S. D. Kempf, and D. D. Blankenship (2013), Weak bed control of the eastern shear margin of Thwaites Glacier, West Antarctica, *J. Glaciol.*, *59*(217), 900–912, doi: 10.3189/2013JoG13J050.

Mader, H. M. (1992), The thermal behaviour of the water-vein system in polycrystalline ice, *J. Glaciol.*, *38*(130), 359–374, doi:10.3189/S0022143000002240.

Marsh, O. J., H. A. Fricker, M. R. Siegfried, K. Christianson, K. W. Nicholls, H. F. J. Corr, and G. Catania (2016), High basal melting forming a channel at the grounding line of Ross Ice Shelf, Antarctica, *Geophys. Res. Lett.*, *43*(1), 250–255, doi:10.1002/2015GL066612.

McKenzie, D. (1984), The generation and compaction of partially molten rock, *J. Petrol.*, *25*(3), 713–765, doi:10.1093/petrology/25.3.713.

Meyer, C. R., and I. J. Hewitt (2017), A continuum model for meltwater flow through compacting snow, *Cryosphere*, *11*(6), 2799–2813, doi:10.5194/tc-11-2799-2017.

Meyer, C. R., M. C. Fernandes, T. T. Creyts, and J. R. Rice (2016), Effects of ice deformation on Röthlisberger channels and implications for transitions in subglacial hydrology, *J. Glaciol.*, *62*(234), 750–762, doi:10.1017/jog.2016.65.

Meyer, C. R., J. W. Hutchinson, and J. R. Rice (2017), The path-independent m integral implies the creep closure of englacial and subglacial channels, *J. Appl. Mech.*, *84*(1), 011,006, doi:10.1115/1.4034828.

Minchew, B., M. Simons, H. Björnsson, F. Pálsson, M. Morlighem, H. Seroussi, E. Larour, and S. Hensley (2016), Plastic bed beneath Hofsjökull ice cap, central Iceland, and the sensitivity of ice flow to surface meltwater flux, *J. Glaciol.*, *62*(231), 147–158, doi: 10.1017/jog.2016.26.

Minchew, B. M., M. Simons, B. V. Riel, and P. Milillo (2017), Tidally induced variations in vertical and horizontal motion on Rutford Ice Stream, West Antarctica, inferred from remotely sensed observations, *J. Geophys. Res.*, *122*, 167–190, doi:10.1002/2016JF003971.

Minchew, B. M., C. R. Meyer, G. H. Gudmundsson, A. A. Robel, and M. Simons (2018), Processes controlling the downstream evolution of ice rheology in glacier shear margins: Case study on Rutford Ice Stream, West Antarctica., *in press J. Glaciol.*, doi: 10.1017/jog.2018.47.

Nereson, N. A. (2000), Elevation of ice-stream margin scars after stagnation, *J. Glaciol.*, *46*(152), 111–118, doi:10.3189/172756500781833241.

Nye, J. F. (1953), The flow law of ice from measurements in glacier tunnels, laboratory experiments and the Jungfraufirn borehole experiment, *Proc. R. Soc. Lond. Ser. A 219*, pp. 477–489, doi:10.1098/rspa.1953.0161.

Nye, J. F. (1976), Water flow in glaciers: jökulhlaups, tunnels and veins, *J. Glaciol.*, *17*(76), 181–207, doi:10.3198/1976JoG17-76-181-207.

Nye, J. F., and F. C. Frank (1973), Hydrology of the intergranular veins in a temperate glacier, in *Symposium on the Hydrology of Glaciers*, vol. 95, pp. 157–161.

Paterson, W. S. B. (1977), Secondary and tertiary creep of glacier ice as measured by borehole closure rates, *Rev. Geophys.*, *15*(1), 47–55, doi:10.1029/RG015i001p00047.

Perol, T., and J. R. Rice (2011), Control of the width of West Antarctic ice streams by internal melting in the ice sheet near the margins, abstract C11B-0677 presented at 2011 Fall Meeting, AGU, San Francisco, Calif., 5-9 Dec.

Perol, T., and J. R. Rice (2015), Shear heating and weakening of the margins of West Antarctic ice streams, *Geophys. Res. Lett.*, *42*(9), 3406–3413, doi:10.1002/2015gl063638.

Perol, T., J. R. Rice, J. D. Platt, and J. Suckale (2015), Subglacial hydrology and ice stream margin locations, *J. Geophys. Res.*, *120*(F003542), 1–17, doi:10.1002/2015jf003542.

Peters, M. E., D. D. Blankenship, and D. L. Morse (2005), Analysis techniques for coherent airborne radar sounding: Application to West Antarctic ice streams, *J. Geophys. Res.*, *110*(B6), 1–17, doi:10.1029/2004JB003222, b06303.

Platt, J. D., T. Perol, J. Suckale, and J. R. Rice (2016), Determining conditions that allow a shear margin to coincide with a Röthlisberger channel, *J. Geophys. Res.*, *121*(7), 1273–1294, doi:10.1002/2015JF003707.

Rathbun, A. P., C. Marone, R. B. Alley, and S. Anandakrishnan (2008), Laboratory study of the frictional rheology of sheared till, *J. Geophys. Res.*, *113*(F2), doi: 10.1029/2007JF000815.

Raymond, C. (1996), Shear margins in glaciers and ice sheets, *J. Glaciol.*, *42*(140), 90–102, doi:10.3198/1996JoG42-140-90-102.

Raymond, C. F., K. A. Echelmeyer, I. M. Whillans, and C. S. M. Doake (2001), Ice stream shear margins, in *The West Antarctic Ice Sheet: Behavior and Environment*, vol. 77, edited by R. B. Alley and R. A. Bindschadler, pp. 157–199, AGU, Washington, DC, doi: 10.1029/ar077p0157.

Raymond, C. F., G. A. Catania, N. Nereson, and C. J. van der Veen (2006), Bed radar reflectivity across the north margin of Whillans Ice Stream, West Antarctica, and implications for margin processes, *J. Glaciol.*, *52*(176), 3–10, doi:10.3189/172756506781828890.

Rempel, A. W. (2008), A theory for ice-till interactions and sediment entrainment beneath glaciers, *J. Geophys. Res.*, *113*(F1), doi:10.1029/2007JF000870, f01013.

Rempel, A. W. (2009), Transient effective stress variations forced by changes in conduit pressure beneath glaciers and ice sheets, *Ann. Glaciol.*, *50*(52), 61–66, doi: 10.3189/172756409789624300.

Rempel, A. W., J. S. Wettlaufer, and M. G. Worster (2004), Premelting dynamics in a continuum model of frost heave, *J. Fluid Mech.*, *498*, 227–244.

Retzlaff, R., and C. R. Bentley (1993), Timing of stagnation of Ice Stream C, West Antarctica, from short-pulse radar studies of buried surface crevasses, *J. Glaciol.*, *39*(133), 553–561, doi:10.3198/1993JoG39-133-553-561.

Rice, J. R. (1967), Stresses due to a sharp notch in a work-hardening elastic-plastic material loaded by longitudinal shear, *J. App. Mech.*, *34*, 287–298, doi:10.1115/1.3607681.

Rice, J. R. (1968), Mathematical analysis in the mechanics of fracture, in *Fracture: An Advanced Treatise (Vol. 2, Mathematical Fundamentals)*, edited by H. Liebowitz, chap. 3, Academic Press, New York.

Röthlisberger, H. (1972), Water pressure in intra- and subglacial channels, *J. Glaciol.*, *11*(62), 177–203, doi:10.3198/1972JoG11-62-177-203.

Scambos, T. A., K. A. Echelmeyer, M. A. Fahnestock, and R. S. Bindschadler (1994), Development of enhanced ice flow at the southern margin of Ice Stream D, Antarctica, *Ann. Glaciol.*, *20*(1), 313–318, doi:10.3198/1994AoG20-1-319-326.

Scambos, T. A., T. M. Haran, M. A. Fahnestock, T. H. Painter, and J. Bohlander (2007), MODIS-based Mosaic of Antarctica (MOA) data sets: Continent-wide surface morphology and snow grain size, *Remote Sens. Environ.*, *111*(2), 242–257, doi: 10.1016/j.rse.2006.12.020.

Schoof, C. (2004), On the mechanics of ice-stream shear margins, *J. Glaciol.*, *50*(169), 208–218, doi:10.3189/172756504781830024.

Schoof, C. (2012), Thermally driven migration of ice-stream shear margins, *J. Fluid Mech.*, *712*, 552–578, doi:10.1017/jfm.2012.438.

Schoof, C., and I. Hewitt (2013), Ice-sheet dynamics, *Ann. Rev. Fluid Mech.*, *45*, 217–239, doi:10.1146/annurev-fluid-011212-140632.

Schoof, C., and I. J. Hewitt (2016), A model for polythermal ice incorporating gravity-driven moisture transport, *J. Fluid Mech.*, *797*, 504–535, doi:10.1017/jfm.2016.251.

Schroeder, D. M., D. D. Blankenship, and D. A. Young (2013), Evidence for a water system transition beneath Thwaites Glacier, West Antarctica, *Proc. Natl. Acad. Sci. U.S.A.*, *110*(30), 12,225–12,228, doi:10.1073/pnas.1302828110.

Schroeder, D. M., H. E. Seroussi, W. Chu, and D. A. Young (2016), Adaptively constraining radar attenuation and temperature across the Thwaites Glacier catchment using bed echoes, *J. Glaciol.*, *62*(236), 1075–1082, doi:10.1017/jog.2016.100.

Smith, B. E., N. E. Lord, and C. R. Bentley (2002), Crevasse ages on the northern margin of Ice Stream C, West Antarctica, *Ann. Glaciol.*, *34*(1), 209–216, doi: 10.3189/172756402781817932.

Suckale, J., J. D. Platt, T. Perol, and J. R. Rice (2014), Deformation-induced melting in the margins of the West Antarctic ice streams, *J. Geophys. Res.*, *119*(5), 1004–1025, doi: 10.1002/2013jf003008.

Truffer, M., and K. A. Echelmeyer (2003), Of isbrae and ice streams, *Ann. Glaciol.*, *36*(1), 66–72, doi:10.3189/172756403781816347.

Tulaczyk, S., W. B. Kamb, and H. F. Engelhardt (2000a), Basal mechanics of Ice Stream B, West Antarctica: 1. till mechanics, *J. Geophys. Res.*, *105*(B1), 463–481, doi: 10.1029/1999JB900329.

Tulaczyk, S., B. Kamb, and H. F. Engelhardt (2000b), Basal mechanics of Ice Stream B, West Antarctica: 2. undrained plastic bed model, *J. Geophys. Res.*, *105*(B1), 483–494, doi:10.1029/1999jb900328.

Vogel, S. (2004), The basal regime of the West-Antarctic Ice Sheet: interaction of subglacial geology with ice dynamics, Ph.D. thesis, University of California Santa Cruz.

Vogel, S. W., S. Tulaczyk, B. Kamb, H. Engelhardt, F. D. Carsey, A. E. Behar, A. L. Lane, and I. Joughin (2005), Subglacial conditions during and after stoppage of an Antarctic Ice Stream: Is reactivation imminent?, *Geophys. Res. Lett.*, *32*, doi:10.1029/2005gl022563.

Werder, M. A., I. J. Hewitt, C. Schoof, and G. E. Flowers (2013), Modeling channelized and distributed subglacial drainage in two dimensions, *J. Geophys. Res.*, *118*(F20146), 1–19, doi:10.1002/jgrf.20146.

Whillans, I. M., and C. J. Van Der Veen (1993), New and improved determinations of velocity of Ice Streams B and C, West Antarctica, *J. Glaciol.*, *39*(133), 483–590, doi: 10.3198/1993JoG39-133-483-490.

Whillans, I. M., and C. J. Van Der Veen (1997), The role of lateral drag in the dynamics of Ice Stream B, Antarctica, *J. Glaciol.*, *43*(144), 231–237, doi:10.3198/1997JoG43-144-231-237.